Journal of Alloys and Compounds 509 (2011) 7742–7748

Contents lists available at ScienceDirect

Journal of Alloys and Compounds

journal homepage: www.elsevier.com/locate/jallcom

Bismuth ferrite bilayered thin films of different constituent layer thicknesses

Jiagang Wu[a,b,*], John Wang[b], Dingquan Xiao[a], Jianguo Zhu[a]

[a] Department of Materials Science, Sichuan University, Chengdu 610064, PR China
[b] Department of Materials Science and Engineering, National University of Singapore, Singapore 117574, Singapore

ARTICLE INFO

Article history:
Received 25 March 2011
Received in revised form 27 April 2011
Accepted 29 April 2011
Available online 10 May 2011

Keywords:
Bismuth ferrite
Bilayer structure
Multiferroic behavior
Fatigue behavior

ABSTRACT

Bilayered thin films consisting of $(Bi_{0.90}La_{0.10})(Fe_{0.85}Zn_{0.15})O_3$ and $(Bi_{0.90}La_{0.10})(Fe_{0.90}Zn_{0.10})O_3$ layers have been fabricated by radio frequency sputtering. Both multiferroic layers are well retained in these bilayers. Their leakage current, multiferroic properties, and fatigue behavior are largely dependent on the thicknesses of $(Bi_{0.90}La_{0.10})(Fe_{0.85}Zn_{0.15})O_3$. With an increase of the thickness in the $(Bi_{0.90}La_{0.10})(Fe_{0.85}Zn_{0.15})O_3$ layer, the leakage current density of bilayers is degraded due to different grain growth modes and an increase in oxygen vacancies, the dielectric constant (ε_r) becomes larger due to the introduction of $(Bi_{0.90}La_{0.10})(Fe_{0.85}Zn_{0.15})O_3$ with a high ε_r value, and their magnetic properties are deteriorated with increasing the thickness ratios of $(Bi_{0.90}La_{0.10})(Fe_{0.85}Zn_{0.15})O_3$ with a weaker magnetization. All bilayers exhibit a good ferroelectric behavior regardless of varying thicknesses of the $(Bi_{0.90}La_{0.10})(Fe_{0.85}Zn_{0.15})O_3$ layer, while their coercive field decreases with increasing the thickness of the $(Bi_{0.90}La_{0.10})(Fe_{0.85}Zn_{0.15})O_3$ layer. An anomalous enhancement in switchable polarization is demonstrated by these bilayers, owing to the involvement of space charges accumulated at the interfaces between two constituent layers.

1. Introduction

Multilayered ferroelectric thin films differing in their structures or/and compositions exhibit novel magnetics [1,2], an improved polarization [3–5], a high dielectric constant [6,7], a new structural phase [8], and other new functional properties [9,10] owing to the epitaxial strain and the interface coupling and interactions among these constituent interfacial layers.

Multiferroic materials have recently attracted much attention [11–24]. Among those, multiferroic $BiFeO_3$ (BFO) material with a rhombohedrally distorted perovskite structure has recently been given to considerable attention due to its giant remanent polarization, a high Curie temperature, and the existence of ferroelectric and ferromagnetic properties at and above room temperature [13–26], and the material shows promise for practical applications in high density ferroelectric random access memories, spintronics, and sensors and actuators, and so on [11–26]. In contrast, a very high leakage current density at room temperature seriously degrades the electrical behavior of BFO material, and thus hinders its practical applications [11–26]. Although some methods have been used to decrease the leakage current density of BFO thin films, their electrical behavior is still not ideal [2,5,27,28]. Among these promising methods, the bilayered structure consisting of BFO and other ferroelectrics may be a more promising method for decreasing the leakage current density and improving the electrical properties of BFO, owing to the advantage of the bilayered structure. In the past, the bilayered thin films consisting of BFO and other ferroelectric layer have been reported [2,5,28], such as $Bi_{1/2}Na_{1/2}TiO_3$, $Pb(Zr, Ti)O_3$. Some interesting results have been demonstrated by such a bilayered structure, such as the reduction in leakage current density, the improvement in phase purity, and the enhancement in fatigue behavior [2,5,26], but their polarization value is much lower as compared with the intrinsic polarization one of BFO thin films [2,5,28].

In the present work, the bilayered thin films consisting of $(Bi_{0.90}La_{0.10})(Fe_{0.85}Zn_{0.15})O_3$ (BLFZO15) and $(Bi_{0.90}La_{0.10})(Fe_{0.90}Zn_{0.10})O_3$ (BLFZO10) layers were grown *in situ* on $Pt/TiO_2/SiO_2/Si(1\,0\,0)$ substrates without any buffer layers by radio frequency (rf) sputtering, where the thickness of the BLFZO10 layer is fixed, and the thickness of the BLFZO15 layer is changed from 20 nm to 180 nm. The thicknesses of the BLFZO15 layer seriously affect the leakage current density, dielectric properties, and multiferroic and fatigue behavior of BLFZO15/BLFZO10 bilayered thin films, and the underlying physics mechanisms were clearly addressed.

2. Experimental procedure

The two-inch BLFZO10 and BLFZO15 ceramic targets with an excess of 10% Bi have been synthesized via a solid state reaction of constituent oxides, namely Bi_2O_3 (99.9%), Fe_2O_3 (99.9%), La_2O_3 (99.99%), and ZnO (99.9%). The powder mixtures of appropriate compositions of these oxides were calcined at ~700 °C in

* Corresponding author at: Department of Materials Science, Sichuan University, Chengdu 610064, PR China. Tel.: +86 28 85412202; fax: +86 28 85412202.
E-mail addresses: wujiagang0208@163.com, msewujg@scu.edu.cn (J. Wu).

0925-8388/$ – see front matter © 2011 Elsevier B.V. All rights reserved.
doi:10.1016/j.jallcom.2011.04.140

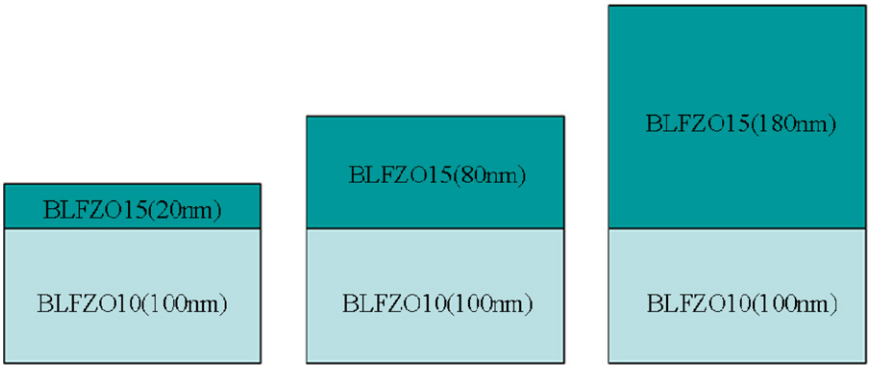

Fig. 1. Diagram for all bilayers.

air for 6 h to form BLFZO10 and BLFZO15 phases, and the BLFZO10 and BLFZO15 green bodies were then sintered at ~820 °C for 2 h to form polycrystalline targets. The BLFZO15/BLFZO10 bilayered thin films were deposited by rf sputtering from BLFZO10 and BLFZO15 ceramic targets. A BLFZO10 layer with a fixed thickness of ~100 nm was firstly deposited on $Pt/TiO_2/SiO_2/Si(1\,0\,0)$ substrates at a substrate temperature of ~550 °C, and then the BLFZO15 layers with different thicknesses of ~20 nm, ~80 nm, ~180 nm were subsequently deposited on $BLFZO10/Pt/TiO_2/SiO_2/Si(1\,0\,0)$ substrates at the substrate temperature of ~530 °C, and the diagram is shown in Fig. 1. The BLFZO15/BLFZO10 bilayered thin films were deposited at an rf power of 120 W, and the rf deposition was carried out at a base pressure of $\sim 10^{-6}$ Torr and a deposition pressure of ~10 mTorr with Ar and O_2 at the ratio of 4:1. For this, circular Au electrodes of diameter 0.2 mm were sputtered on the film surface using a shadow mask in order to investigate the electrical properties of these films. The phase structure in these bilayers was analyzed by using X-ray diffraction (Bruker D8 Advanced XRD, Bruker AXS Inc., Madison, WI, CuKa). Their dielectric behavior was characterized by an impedance analyzer (Solartron Grain Phase Analyzer). Their fatigue and ferroelectric properties were studied by using the Radiant precise workstation (Radiant Technologies, Medina, NY). Magnetic behavior of bilayers was characterized using Superconducting Quantum Interference Devices (SQUID, MPMS, XL-5AC, San Diego, CA).

3. Results and discussion

3.1. Structural analysis

Fig. 2(a) shows the XRD patterns of bilayers, together with BLFZO10 and BLFZO15 single layers. The pure phase is demonstrated for all thin films when deposited on Pt-coated silicon substrates without any buffer layers, and no secondary phases are detected except for the substrate peaks. Secondary phases often form in the BFO thin films often have a formation of secondary phases when directly deposited on Pt-coated silicon substrates without any buffer layers [2,5]. Therefore, the La and Zn co-substitutions in the present work improve the phase purity of BFO thin films. In addition, all bilayers exhibit a (1 1 0) orientation due to the induced growth of the bottom BLFZO10 layer with a (1 1 0) orientation, as plotted in Fig. 2(a). Fig. 2(b) indicates the enlarged XRD patterns in the 2θ range of 31–33° for all thin films, where the peaks were simulated by the Lorentzian method. The phases of BLFZO10 and BLFZO15 layers are well retained in those bilayers.

All bilayers appear dense and crack-free in surface morphologies, as shown by SEM micrographs. Fig. 3(a)–(c) shows the SEM patterns for the bilayers with different thicknesses of the BLFZO15 layer. Some black and white regions are observed for the surface morphologies of all bilayers. To further characterize the grain growth mode in these black and white regions, an enlarged SEM pattern was taken, as shown in Fig. 3(d). The black and white regions represent the different grain growth modes, that is, the black regions represent the grain growth parallel to substrate, and the white ones represent the grain growth vertical to substrate. Moreover, some small pores among grains are found for these white regions, while the surface morphology is very dense for the black ones. Therefore, the 20BLFZO15/100BLFZO10 bilayer possesses more black regions as compared with those of the 80BLFZO15/100BLFZO10 and 180BLFZO15/100BLFZO10 bilayers,

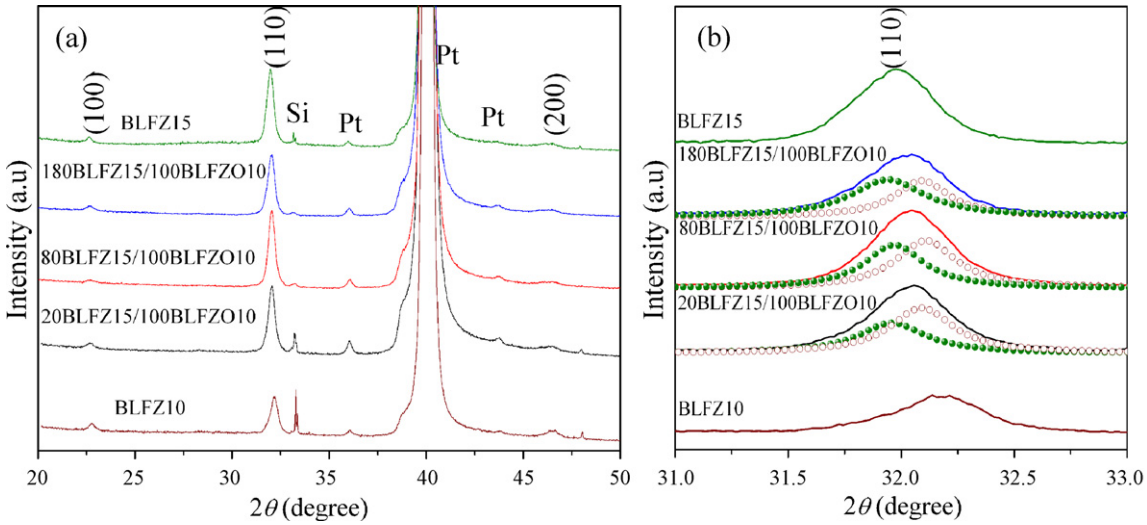

Fig. 2. (a) XRD patterns of all bilayers, together with BLFZO10 and BLFZO15 single layers. (b) Enlarged XRD patterns in the 2θ range of 31–33° for all thin films.

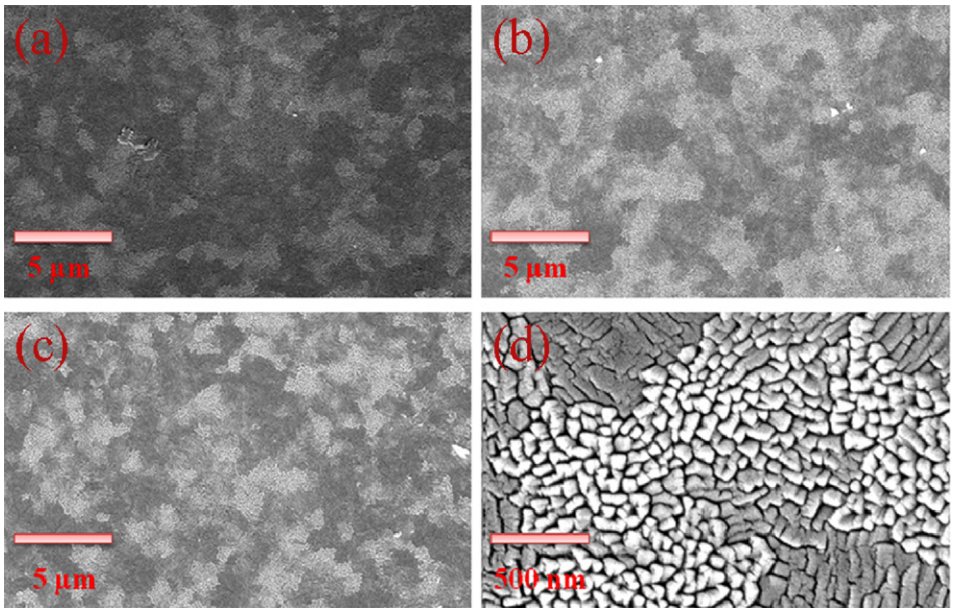

Fig. 3. SEM patterns for the (a) 20BLFZO15/100BLFZO10, (b) 80BLFZO15/100BLFZO10, and (c) 180BLFZO15/100BLFZO10 bilayers. (d) Enlarged SEM patterns for these bilayers.

indicating that the 20BLFZO15/100BLFZO10 bilayer has the denser microstructure.

3.2. Leakage analysis

Fig. 4(a) shows the *J–E* curves for all bilayers, measured at room temperature. The 80BLFZO15/100BLFZO10 and 180BLFZO15/100BLFZO10 bilayers exhibit a similar leakage current behavior, while a much lower leakage current density is observed for the 20BLFZO15/100BLFZO10 bilayers. The leakage current density is related to the surface morphologies of these bilayers, where the denser microstructure is well established for the 20BLFZO15/100BLFZO10 bilayer, as shown in Fig. 3(a). Moreover, the Zn^{2+} substitution for the Fe^{3+} site in BFO generates more oxygen vacancies [29], where the oxygen vacancies should dominate the leakage behavior of BFO thin films. For the BLFZO10 thin film, the La substitution for the Bi site helps suppress the formation of oxygen vacancies, and thus a lower leakage current

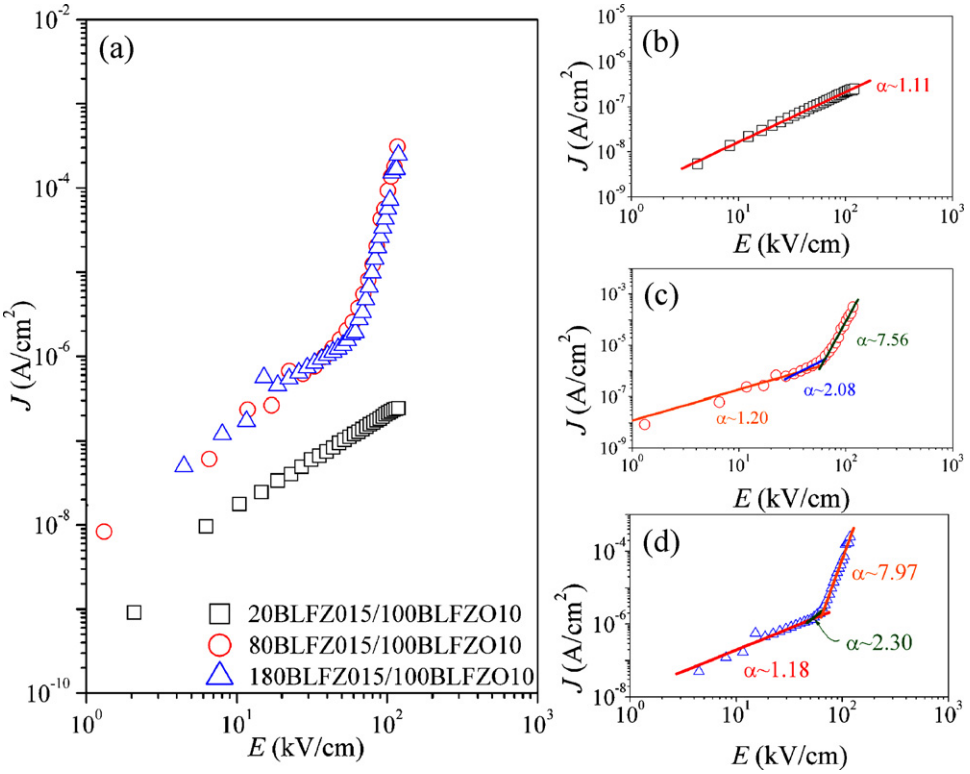

Fig. 4. (a) *J–E* curves for the BLFZO15/BLFZO10 bilayers. The *log–log* plots of the leakage current density of (b) 20BLFZO15/100BLFZO10, (c) 80BLFZO15/100BLFZO10, and (d) 180BLFZO15/100BLFZO10 bilayers.

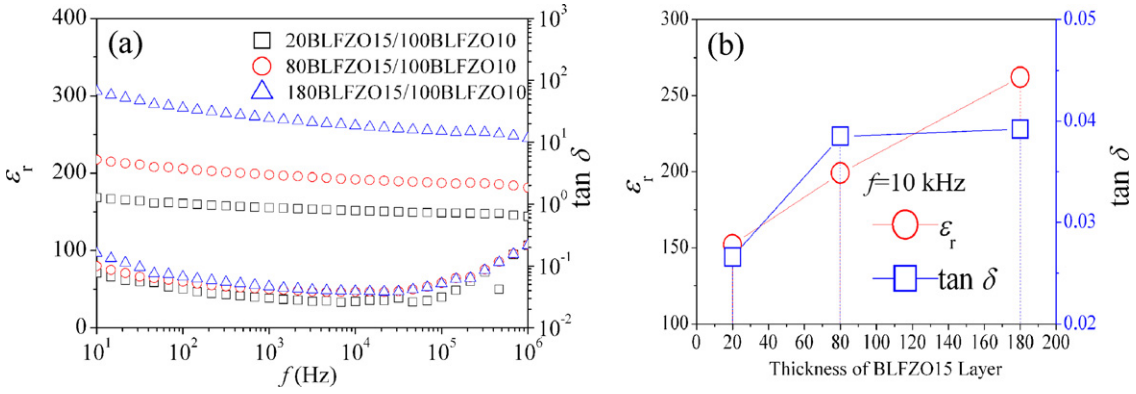

Fig. 5. (a) Dielectric behavior of all bilayers. (b) Dielectric constant and dielectric loss as a function of the BLFZO15 layer thicknesses at 10 kHz.

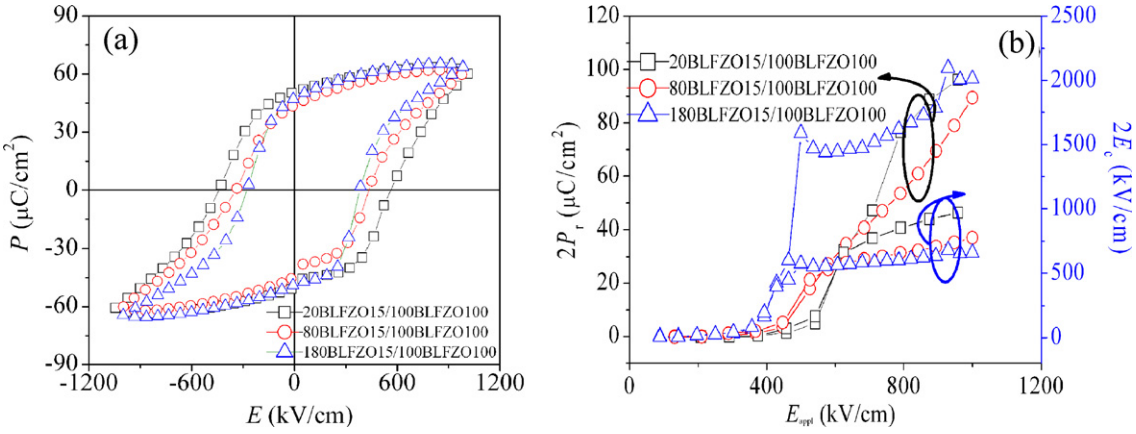

Fig. 6. (a) Ferroelectric properties of all bilayers. (b) $2P_r$ and $2E_c$ values of all bilayers as a function of applied electric fields.

density is observed. While the Zn^{2+} substitution for the Fe site dominates the leakage behavior for the BLFZO15 thin film, a higher leakage current density is demonstrated. Therefore, the leakage current of BLFZO15/BLFZO10 bilayers is degraded with an increase in the thickness of the BLFZO15 layer. As shown in Fig. 4(b), the leakage current of the 20BLFZO15/100BLFZO10 bilayer appears to increase almost linearly, with a slope close to the unity, indicating the involvement of an Ohmic conduction. However, the 80BLFZO15/100BLFZO10 and 180BLFZO15/100BLFZO10 bilayers have a similar leakage mechanism, while their leakage mechanisms are obviously different from that of the 20BLFZO15/100BLFZO10 bilayer, and the *log–log* plots of the leakage current density vs. applied electric field are shown in Fig. 4(b)–(d). The leakage current curves can be divided into several regions according to the SCLC theory [30], where the slope ($\alpha \sim \log J/\log E$) of each region can be fitted. At low electric fields, an Ohmic conduction behavior is demonstrated. With an increase in applied electric fields, a rather different conduction process is initiated, and the leakage current density largely follows a square dependence on applied electric fields ($\alpha \sim 2$), which corresponds to the Child's law region. In the Child's law region, the concentration of free electrons due to carrier injection greatly exceeds the equilibrium concentration in BFO thin film, and contributes to an increase in leakage current density. With a further increase in applied electric fields, a dramatic increase

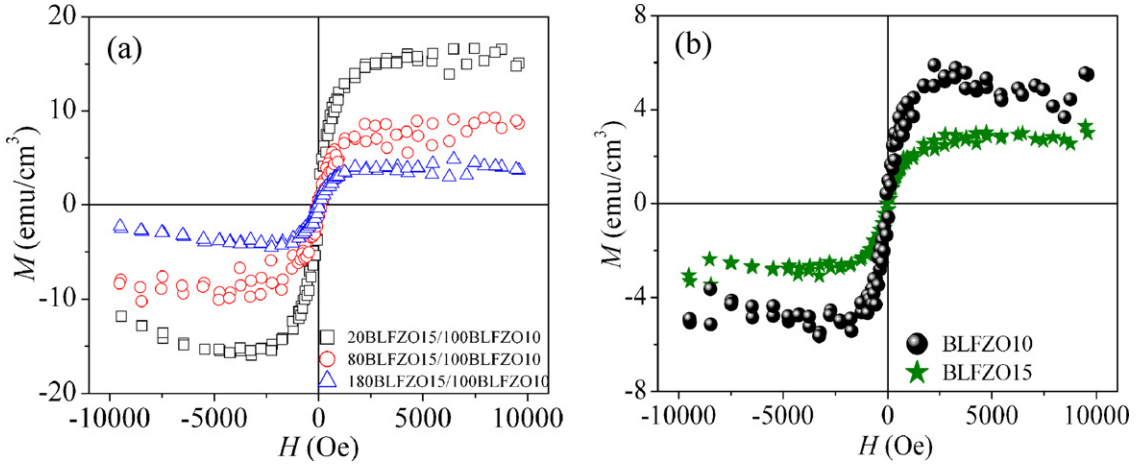

Fig. 7. *M–H* loops of (a) all bilayers and (b) BLFZO15 and BLFZO10 single layers.

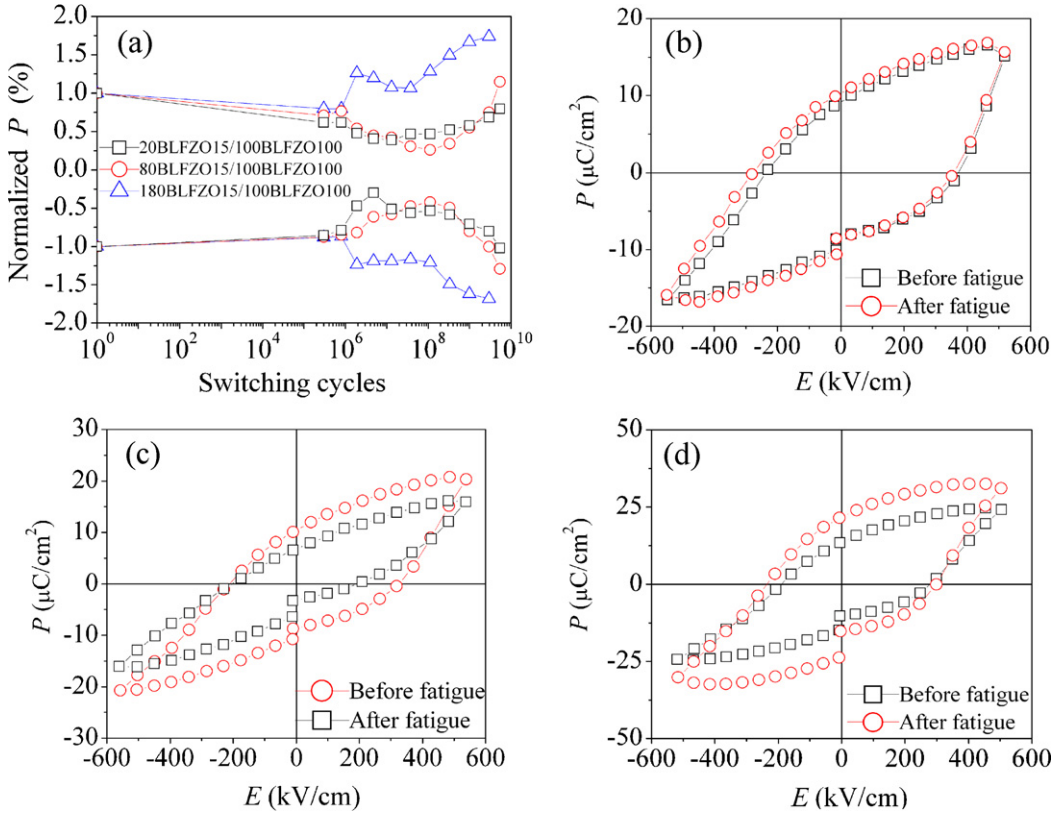

Fig. 8. (a) Fatigue behavior of all bilayers. *P–E* curves before and after fatigue for (b) 20BLFZO15/100BLFZO10, (c) 80BLFZO15/100BLFZO10, and (d) 180BLFZO15/100BLFZO10 bilayers.

in leakage current occurs due to the interaction between the positively charged traps and electrons obeying the trap-filled-limit law. Therefore, the conduction behavior of 80BLFZO15/100BLFZO10 and 180BLFZO15/100BLFZO10 bilayers obeys the SCLC theory, while an Ohmic conduction is involved into the 20BLFZO15/100BLFZO10 bilayer.

3.3. Dielectric properties

The dielectric behavior of all bilayers as a function of frequencies of $\sim 10^1$–10^6 Hz was characterized, as plotted in Fig. 5(a). The dielectric constant (ε_r) increases with an increase in the thickness of the BLFZO15 layer, due to the introduction of the BLFZO5 layer with a higher ε_r value. A lower dielectric loss ($\tan\delta$) is observed for 20BLFZO15/100BLFZO10 as compared with those of 80BLFZO15/100BLFZO10 and 180BLFZO15/100BLFZO10 bilayers, confirming the involvement of a lower free movable charge concentration in the 20BLFZO15/100BLFZO10 bilayer [31]. This result is in agreement with the dense microstructure in Fig. 3 and the leakage behavior in Fig. 4. Fig. 5(b) plots the ε_r and $\tan\delta$ values as a function of the BLFZO15 layer thicknesses at 10 kHz. These results also clearly illuminate that the ε_r value linearly increases with increasing the thickness of the BLFZO15 layer, and a lower $\tan\delta$ value is formed in the 20BLFZO15/100BLFZO10 bilayer.

3.4. Ferroelectric behavior

Fig. 6(a) plots the *P–E* hysteresis loops of all bilayers, measured at 5 kHz and room temperature. All bilayers have similarly saturated remanent polarization ($2P_r$) values regardless of varying thicknesses of the BLFZO15 layer. In contrast, their coercive field ($2E_c$) values exhibit obviously different from each other, and decrease with increasing the thicknesses of the BLFZO15 layer, where the 180BLFZO15/100BLFZO10 bilayer has a lowest $2E_c$ value among those bilayers. Fig. 6(b) plots the $2P_r$ and $2E_c$ values for all bilayers as a function of applied electric fields. The 180BLFZO15/100BLFZO10 bilayer easily reaches a saturation in $2P_r$ and $2E_c$ values, where the $2P_r$ and $2E_c$ values slowly change when the applied electric field is more than ~450 kV/cm. Moreover, it is also clearly observed from Fig. 6(b) that a lower $2E_c$ value of ~658.93 kV/cm is demonstrated for the 180BLFZO15/100BLFZO10 bilayer, together with a well saturated ferroelectric behavior. The $2P_r \sim 96.5\ \mu C/cm^2$ value of the 180BLFZO15/100BLFZO10 bilayer is larger than those of BFO-based bilayers reported by other authors [2,5,28]. The enhancement in $2P_r$ value of bilayers in this work should be attributed to a (110) orientation and a high phase purity, together with an interface coupling and reaction between BLFZO10 and BLFZO15 layers.

3.5. Magnetic behavior

Fig. 7(a) plots the *M–H* curves of all bilayers, measured at room temperature. The saturated *M–H* loops are observed for all bilayers, while the thickness of the BLFZO15 layer strongly affects the saturation magnetizations (M_s) values of BLFZO15/BLFZO10 bilayers, that is, their M_s values are degraded with an increase in the thickness of the BLFZO15 layer. To clearly explain this phenomenon, the *M–H* curves of BLFZO10 and BLFZO15 single layers were measured at room temperature, and plotted in Fig. 7(b). As shown in Fig. 7(b), the BLFZO15 single layer has a lower M_s value than that of the BLFZO10 single layer due to the increase in the nonmagnetic Zn composition. Therefore, the decrease in M_s value with increasing BLFZO15 layer thicknesses should be attributed to the worse magnetic properties in the BLFZO15 layer. In addition, the 20BLFZO15/100BLFZO10 bilayer has a high $2M_s$ value of ~30.6 emu/cm^3, which is higher than those of BFO single layers and bilayers reported before [5,28,32]. The enhancement in

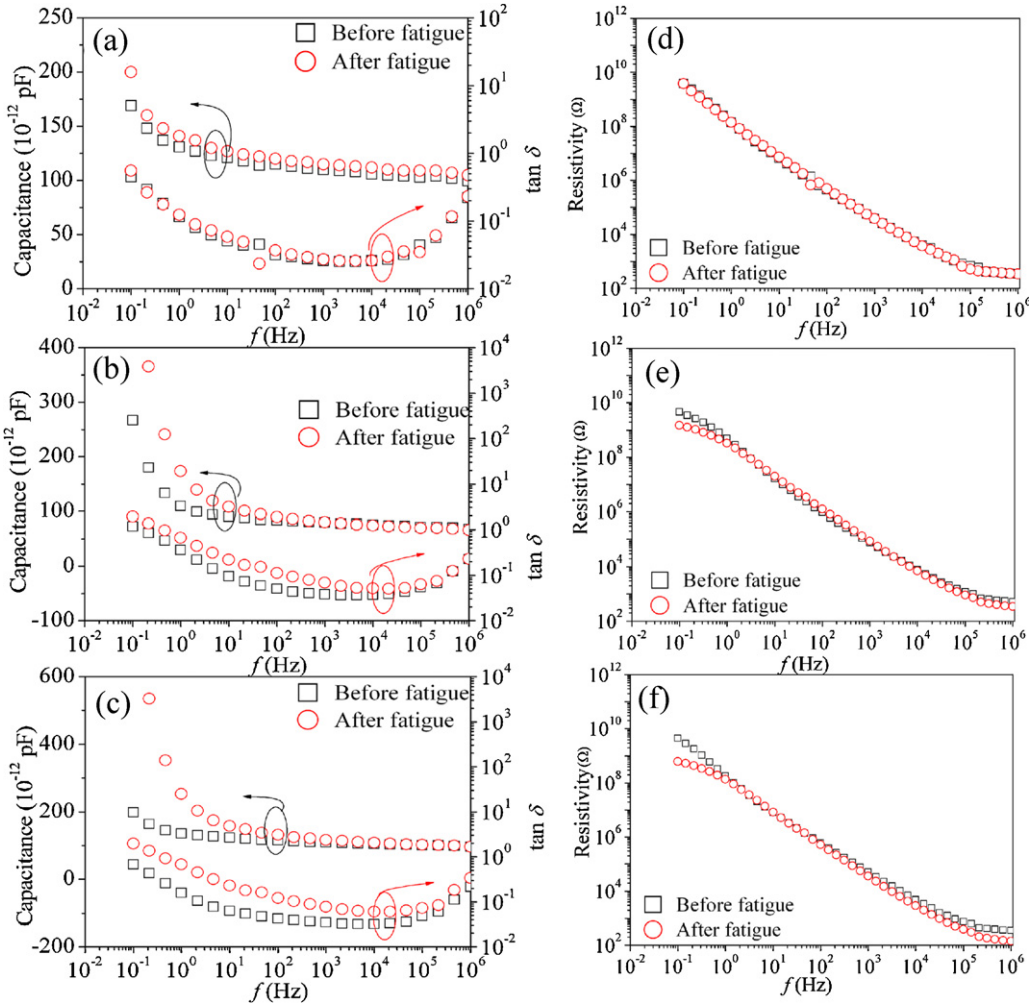

Fig. 9. (a) Capacitance vs. frequency before and after fatigue of (a) 20BLFZO15/100BLFZO10, (b) 80BLFZO15/100BLFZO10, and (c) 180BLFZO15/100BLFZO10 bilayers. Resistivity vs. frequency before and after fatigue for (d) 20BLFZO15/100BLFZO10, (e) 80BLFZO15/100BLFZO10, and (f) 180BLFZO15/100BLFZO10 bilayers.

magnetization behavior of the 20BLFZO15/100BLFZO10 bilayer is attributed to the decrease in the BLFZO15 layer thickness with a lower M_S value and the interface coupling between BLFZO15 and BLFZO10 layers.

3.6. Fatigue behavior

Fig. 8(a) shows the fatigue behavior of all bilayers as a function of switching cycles, measured at the frequency of 100 kHz and an applied electric field of ~542 kV/cm. The unusual fatigue behavior is observed for all bilayers, that is, the polarization value is firstly degraded, and then is improved with increasing the switching cycles. In order to illuminate the unusual fatigue behavior, the *P–E* loops before and after fatigue were also measured for all bilayers, as plotted in Fig. 8(b)–(d). The polarization value slightly increases for the 20BLFZO15/100BLFZO10 bilayer, while the polarization values dramatically increase after the fatigue switching cycles for the 80BLFZO15/100BLFZO10 and 180BLFZO15/100BLFZO10 bilayers, together with a roundish *P–E* loop. These results in Fig. 8(b)–(d) are in agreement with the fatigue behavior [Fig. 8(a)]. Usually, it is well known that the space charge and defect concentration dominate the fatigue behavior of multilayered thin films [2,33,34]. To identifying whether these factors affect the fatigue behavior of all bilayers in present work, the dielectric behavior and resistivity before and after fatigue were characterized, as shown in Fig. 9. For the 20BLFZO15/100BLFZO10 bilayer, the dielectric constant, dielectric loss, and resistivity almost keep unchanged after the fatigue switching cycles, indicating the involvement of few space charge and defects during switching cycles. In contrast, the dielectric constant and loss of 80BLFZO15/100BLFZO10 and 180BLFZO15/100BLFZO10 bilayers increase in a low-frequency region of $\sim 10^{-1}$–10^{1} Hz, and the resistivity decreases, dependent on the BLFZO15 layer thickness, confirming the involvement of more space charge and higher defects concentration during switching cycles. High capacitance at low frequency (<10 Hz) in Fig. 9(b) and (c) is due to the conductivity in the sample [35], and agrees with higher tan δ and low resistivity of fatigued sample. Therefore, the space charge should be responsible for the unusual fatigue behavior in 80BLFZO15/100BLFZO10 and 180BLFZO15/100BLFZO10 bilayers, while the space charge is few involved into the 20BLFZO15/100BLFZO10 bilayer.

4. Conclusion

$(Bi_{0.90}La_{0.10})(Fe_{0.85}Zn_{0.15})O_3/(Bi_{0.90}La_{0.10})(Fe_{0.90}Zn_{0.10})O_3$ bilayers have been grown on Pt-coated silicon substrates without any buffer layers by radio frequency sputtering. Both BLFZO15 and BLFZO10 phases are well retained in these bilayers. The dielectric constant of bilayers increases with an increase in the thickness of the BLFZO15 layer, owing to the introduction of the BLFZO15 layer with a large dielectric constant. The *P–E* hysteresis loops are well saturated with a large polarization value for all bilayers, while their coercive field decreases with increasing the thicknesses fraction

of the BLFZO15 layer. An anomalous enhancement in switchable polarization is demonstrated by the bilayers, which is related to the space charges that are accumulated at the interfaces between BLFZO15 and BLFZO10 layers.

Acknowledgement

Dr. Jiagang Wu gratefully acknowledges the supports of the introduction of talent start funds of Sichuan University (2082204144033), the Sichuan University, and the National University of Singapore. Thank reviewers and editor for their good comments and advice, which benefit to the improvement of our paper.

References

[1] S.S.P. Parkin, C. Kaiser, A. Panchula, P.M. Rice, B. Hughes, M. Samant, S.H. Yang, Nat. Mater. 3 (2004) 862.
[2] J.G. Wu, G.Q. Kang, H.J. Liu, J. Wang, Appl. Phys. Lett. 94 (2009) 172906.
[3] H.N. Lee, H.M. Christen, M.F. Chisholm, C.M. Rouleau, D.H. Lowndes, Nature 433 (2005) 395.
[4] I. Vrejoiu, Y. Zhu, G.L. Rhun, M.A. Schubert, D. Hesse, M. Alexe, Appl. Phys. Lett. 90 (2007) 072909.
[5] J.G. Wu, G.Q. Kang, J. Wang, Appl. Phys. Lett. 95 (2009) 192901.
[6] Z.H. Zhou, J.M. Xue, W.Z. Li, J. Wang, H. Zhu, J.M. Miao, J. Appl. Phys. 96 (2004) 5706.
[7] J.G. Wu, D.Q. Xiao, J.G. Zhu, J.L. Zhu, J.Z. Tan, Q.L. Zhang, Appl. Phys. Lett. 90 (2007) 082902.
[8] V.R. Cooper, K. Johnston, K.M. Rabe, Phys. Rev. B 76 (2007) 020103.
[9] N. Reyren, S. Thiel, A.D. Caviglia, L.F. Kourkoutis, G. Hammerl, C. Richter, C.W. Schneider, T. Kopp, A.S. Ruetschi, D. Jaccard, M. Gabay, D.A. Muller, J.M. Triscone, J. Mannhart, Science 317 (2007) 1196.
[10] M. Dawber, N. Stucki, C. Lichtensteiger, S. Gariglio, P. Ghosez, J.M. Triscone, Adv. Mater. 19 (2007) 4153.
[11] R. Ramesh, Nature 461 (2009) 1218.
[12] N. Mathur, Nature 454 (2008) 591.
[13] G. Catalan, J.F. Scott, Adv. Mater. 21 (2009) 2463.
[14] L.W. Martin, Y.H. Chu, R. Ramesh, Mater. Sci. Eng. R 68 (2010) 89.
[15] K.F. Wang, J.M. Liu, Z.F. Ren, Adv. Phys. 58 (2009) 321.
[16] C.W. Nan, M.I. Bichurin, S.X. Dong, D. Viehland, G. Srinivasan, J. Appl. Phys. 103 (2008) 031101.
[17] A. Belik, H. Yusa, N. Hirao, Y. Ohishi, E. Takayama-Muromachi, Chem. Mater. 21 (14) (2009) 3400.
[18] J. Chen, X. Xing, A. Watson, W. Wang, R. Yu, J. Deng, L. Yan, C. Sun, X. Chen, Chem. Mater. 19 (15) (2007) 3598.
[19] S.M. Selbach, T. Tybell, M.-A. Einarsrud, T. Grande, Chem. Mater. 19 (26) (2007) 6478.
[20] M. Valant, A.-K. Axelsson, N. Alford, Chem. Mater. 19 (22) (2007) 5431.
[21] W. Chen, A.J. Williams, L. Ortega-San-Martin, M. Li, D.C. Sinclair, W. Zhou, J.P. Attfield, Chem. Mater. 21 (10) (2009) 2085.
[22] S. Ryu, J.-Y. Kim, Y.-H. Shin, B.-G. Park, J.Y. Son, H.M. Jang, Chem. Mater. 21 (21) (2009) 5050.
[23] C.-J. Cheng, A.Y. Borisevich, D. Kan, I. Takeuchi, V. Nagarajan, Chem. Mater. 22 (8) (2010) 2588.
[24] J. Wu, J. Wang, J. Phys. Chem. C 114 (45) (2010) 19318.
[25] F. Yan, M.O. Lai, L. Lu, T.J. Zhu, J. Phys. Chem. C 114 (15) (2010) 6998.
[26] H. Béa, M. Bibes, S. Fusil, K. Bouzehouane, E. Jacquet, K. Rode, P. Bencok, A. Barthélémy, Phys. Rev. B. 74 (2006) 020101(R).
[27] H.Y. Zhao, H. Kimura, Z.X. Cheng, X.L. Wang, T. Nishida, Appl. Phys. Lett. 95 (2009) 232904.
[28] D. Xie, Y. Zang, Y. Luo, X. Han, T. Ren, L. Liu, J. Appl. Phys. 105 (2009) 084109.
[29] X.D. Qi, J. Dho, R. Tomov, M.G. Blamire, J.L. MacManus-Driscoll, Appl. Phys. Lett. 86 (2005) 062903.
[30] M.A. Lampert, Phys. Rev. 103 (1956) 1648.
[31] Z.X. Cheng, X.L. Wang, S.X. Dou, H. Kimura, K. Ozawa, Phys. Rev. B 77 (2008) 092101.
[32] J.G. Wu, J. Wang, Electrochem. Solid-State Lett. 13 (2010) G68.
[33] C.H. Sim, H.P. Soon, Z.H. Zhou, J. Wang, Appl. Phys. Lett. 89 (2006) 122905.
[34] Q.Y. Jiang, E.C. Subbarao, L.E. Cross, J. Appl. Phys. 75 (1994) 7433.
[35] C.R. Bowen, D.P. Almond, Mater. Sci. Technol. 22 (2006) 719.